Effect of plastic deformation and boundary conditions combined with elastic wave propagation on the collapse site of a crash box

A. Rusinek[a,*], R. Zaera[b], P. Forquin[a], J.R. Klepaczko[a]

[a]*Laboratory of Physics and Mechanics of Materials, UMR CNRS 75 54, University Paul Verlaine of Metz, Ile du Saulcy, 57045 Metz cedex, France*
[b]*Department of Continuum Mechanics and Structural Analysis, University Carlos III of Madrid, Avda. de la Universidad 30, 28911 Leganés, Madrid, Spain*

Abstract

Several papers have been published recently on the crashworthiness studies. The main task was to predict the energy absorption W_p and average collapse force $\bar{F}$ in time of sheet steel structures. The main objective of this contribution is to design a component that allows absorbing and dissipating a high energy W_p allowing improvements of the survivability of passengers in vehicles. However, the range of applications is larger since it includes all civil and military applications related to safety of components, or more generally of construction elements being loaded by impacts or explosions. In the present 3D case, the aim of this numerical study on dynamic loading in adiabatic conditions of deformation is to analyze the effect of elastic wave propagation combined with plastic behavior on the collapse site of a rectangular tubular structure made of steel sheet. To demonstrate the strong coupling between the effects of strain rate sensitivity, accounted for in the constitutive relation that is used in numerical simulations, with the process of elastic wave reflection on the boundary conditions, a series of numerical simulation was performed. It is shown in this numerical study that the strain rate sensitivity influences the position of the first collapse site. Moreover, the first collapse initiation of a structure defines the level of power absorption. Since the process of folding may be combined with bending of the structure (in particular when a local buckling appears close to the opposite side of impact), in this non axial case the energy absorption W_p decreases and the effectiveness of the structure to the energy absorption is insufficient.

Keywords: Crashworthiness; Collapse of a steel crash box; Numerical simulation; Plasticity; Elastic waves

1. Introduction

Steel sheets of relatively high strength are currently used in automotive industry, to enhance the energy absorption of components like a crash box, Fig. 1(a). The task of this kind of structure is to absorb a high energy during an accident, mainly in order to assure security of passengers by limiting the maximum deceleration level. Therefore, the structure must deform by a process of collapse and sequential folding during plastic deformation. During the collapse of the structure, in the present case the "crash box", the process of plastic deformation must be controlled. This kind of structures is frequently used in front of the car or laterally as shown in Fig. 3(b) to protect passengers and driver. This type of structure has a history of plastic deformation during metalworking, which affects also the response during a crash. Sheets after rolling pass several operations with different paths of loading, Fig. 1(b), such as tension, bending and stretching, which are carried out at different strain rates, Figs. 1(b) and 2. Thus the dynamic response of the crash box is affected by the history of pre-plastic deformation induced to the assumed hat shape constituting the crash box [1]. The rate effects (the velocity of forming) used during the manufacturing operations contributes also. In this work a particular attention is focused to the strain-rate sensitivity, in addition to the strain hardening as reported in [2].

Fig. 1(b) defines the domain of strain paths of a sheet at different strain rates and also for different values of friction coefficient μ ($\mu = 0$, bi-axial loading). It can be observed that high values of the effective plastic strain rate $\dot{\varepsilon}^p$ induce

*Corresponding author.
E mail address: rusinek@lpmm.univ metz.fr (A. Rusinek).

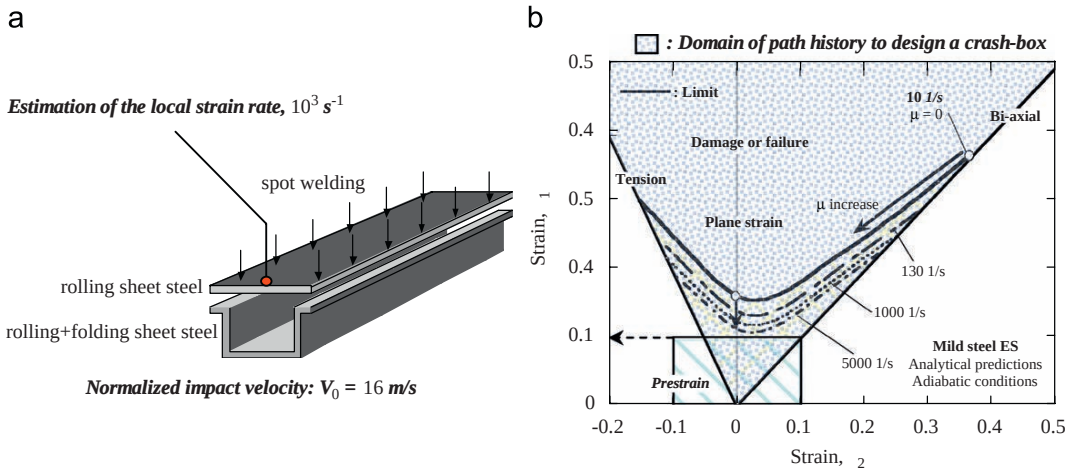

Fig. 1. (a) Schematic representation of the process of crash box fabrication; (b) analytic prediction of forming limit diagram (FLD) for mild steel ES in adiabatic conditions for different strain rates [40].

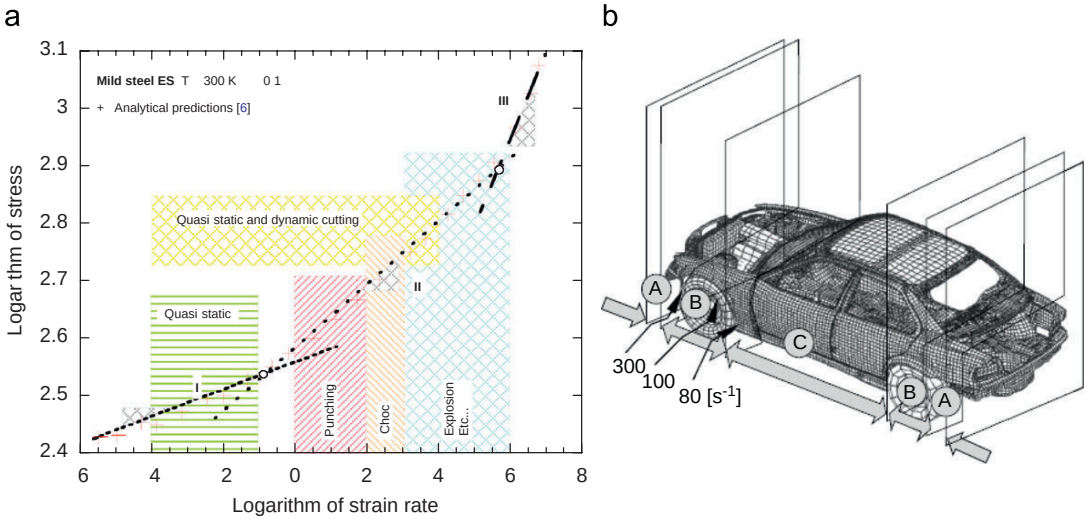

Fig. 2. (a) Strain rate sensitivity for crash test application, ES steel (mild steel); (b) estimation of the strain rate during a crash test [14,45].

a substantial decrease of the strain limit due to adiabatic heating. However for $\dot{\varepsilon} = 10^2\,\mathrm{s}^{-1}$, which corresponds to the strain rate limit observed in punching, Fig. 2, the strain level is more or less equal to the value observed in quasi-static deformation. Moreover, the plastic pre-deformation imposed is always lower than 10% [3], Fig. 1(b). The knowledge of deformation history is important for new materials such as transformation induced by plasticity (TRIP) steel since the process of pre-deformation induces a phase transformation which affects at the same time the mechanical properties of structure [4–6]. For this material during the process of punching the initial residual austenite, which is always present, transforms into martensite, which is a hard phase in comparison with ferrite and austenite [4]. Therefore the level of effective stress σ is affected at the same time by the rate of strain hardening ($n = \partial \log \sigma / \partial \log \varepsilon$). These new materials are used more frequently, Fig. 3(b), to increase the energy absorption of structures, in complement of dual phase (DP) or high strength low alloy (HSLA) steels.

In this study, however, the most popular steel is considered: the mild steel, Fig. 3(a). This material was studied because several tension tests have been performed in quasi-static conditions and in relatively high strain rates allowing for a good recognition of its behavior in terms of strain hardening, including strain rate and temperature sensitivity [7–11], Fig. 4(a). The isotropic plastic behavior showed by this material allows the usage of an isotropic plasticity theory in its modeling.

In addition to the analysis of experimental results, a thermo-visco-plastic model in 3D has been applied to predict the behavior of this material for wide ranges of strain rate and temperature [7,12]. The model has allowed obtaining good predictions for different kinds of applications. Verification is

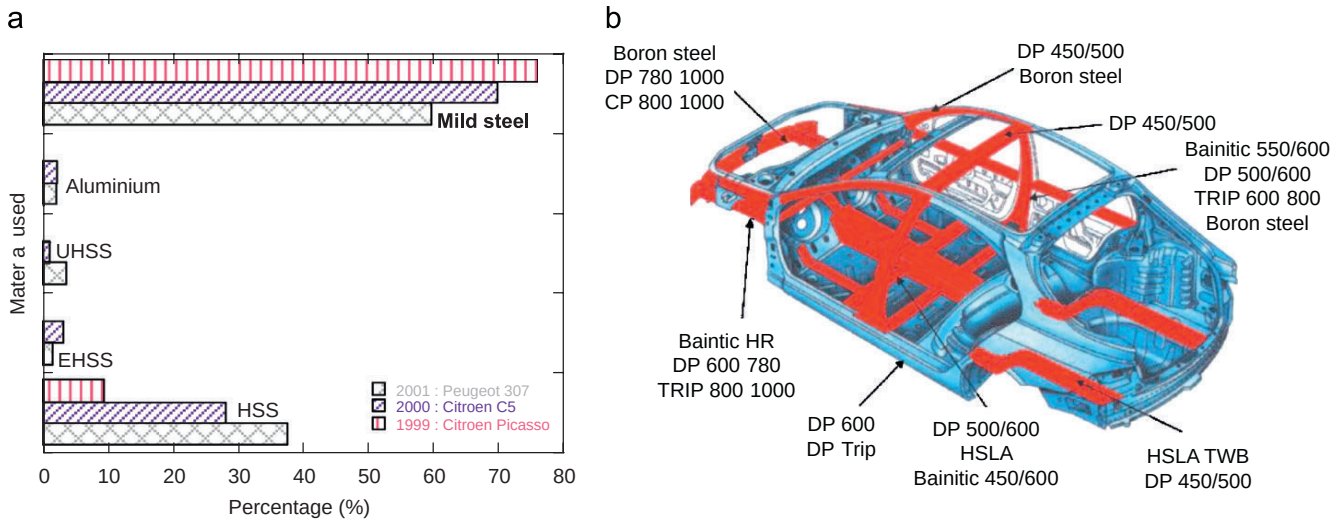

Fig. 3. (a) Percentage of steel used in a car in comparison with aluminum [41]; (b) definition of different safety components assimilated as crash box during numerical simulation [42].

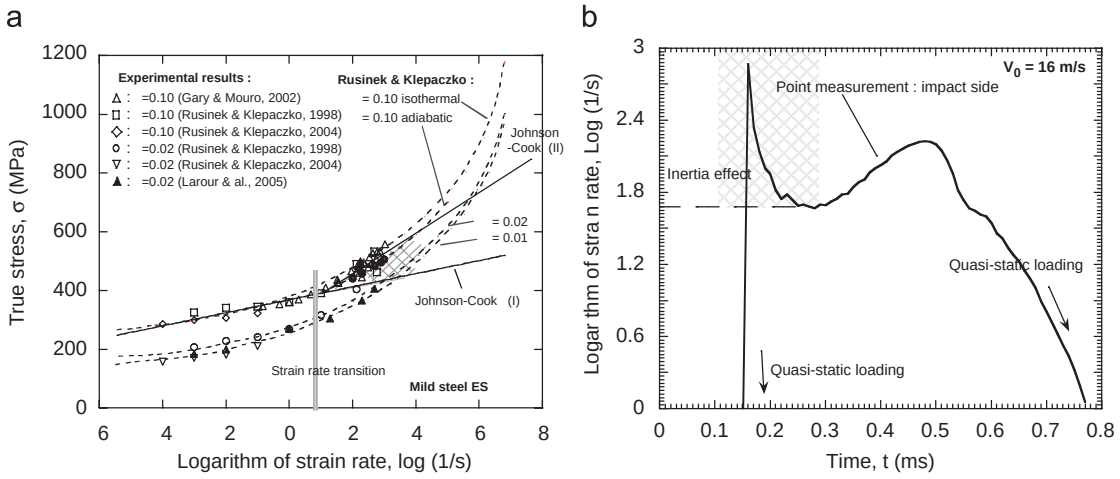

Fig. 4. (a) Strain rate sensitivity of mild steel ES, comparison between experiments and analytical predictions. (b) Estimation of the local strain rate (point Fig. 1a) during crash test.

demonstrated in Fig. 4(a), in terms of different strain rates. The problem with the crash-box simulation is generally related to the fact that the average effective plastic strain rate $\dot{\varepsilon}^{p}$, Fig. 4(b), corresponds exactly to the loss of linearity of the plot in $(\sigma - \log \dot{\varepsilon}^{p})$ coordinates. The strain-rate sensitivity for mild steels begins to increase at strain rate around $10\,s^{-1}$, Fig. 4(a).

It is clear that the usage of constitutive relation with linear strain-rate sensitivity such as in the Johnson–Cook constitutive relation will affect the predictions of energy absorption. If the equation is fitted for the low strain rates range, a large error in the stress level appears at the impact side of the crash box where $\dot{\varepsilon}^{p} \approx 10^{3}\,s^{-1}$. This occurs during the first stage of impact. If the JC constitutive equation is fitted for the high strain rates range, the stress level will be under-estimated as soon the loading goes on and $\dot{\varepsilon}^{p}$ decreases and stabilizes around low average value, Fig. 4(b) [13,14]. It is therefore necessary to apply a reliable approximation of the visco-plastic behavior for a wide range of strain rates. Of course, such improvement must be coupled with the temperature effect that takes place in dynamic loading. Indeed, such range of strain rates $100 \leqslant \dot{\varepsilon}^{p} \leqslant 10^{3}\,s^{-1}$ is above transition from the isothermal process to adiabatic heating. The adiabatic heating is related to a thermal softening of the material. The thermal softening accelerates all plastic instabilities, modifies the rate of strain hardening and, consequently, the process of plastic wave propagation. This effect is amplified at low temperatures. It is shown by the σ–ε curves in Fig. 5(b), for strain rate $10^{-1}\,s^{-1}$, that the strain hardening rate decreases at low temperature but not in the case of strain rate $10^{-4}\,s^{-1}$. This occurs because the isothermal to adiabatic

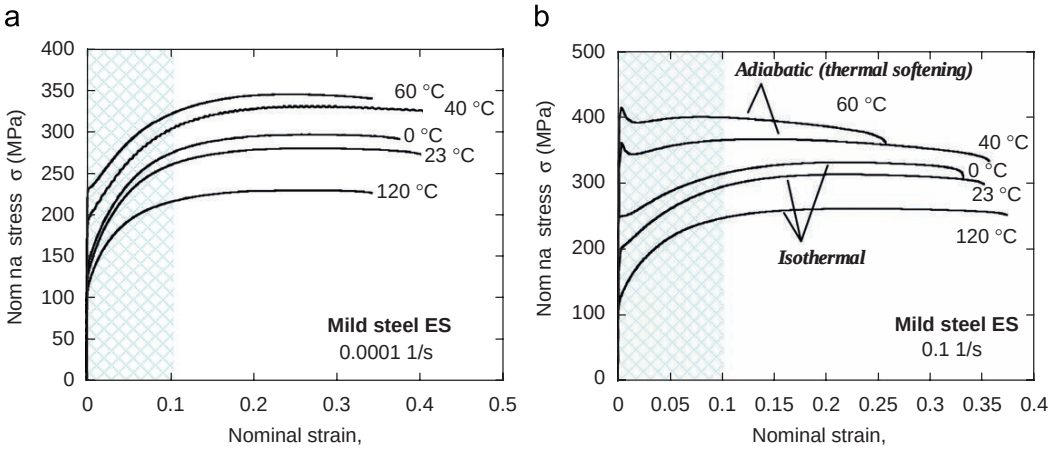

Fig. 5. Effect of initial temperature and strain rate on the hardening of ES steel: (a) $10^{-4}\,s^{-1}$ and (b) $10^{-1}\,s^{-1}$.

transition is not yet reached. In the case of $\dot{\varepsilon}^p = 10^{-4}\,s^{-1}$, the change in strain hardening rate is less important in comparison with strain rate $10^{-1}\,s^{-1}$. Thus, during an accident in winter conditions this effect must be considered and not neglected. In summer, such effect will be delayed since the strain-rate transition will be at higher strain rate. Summarizing, to analyze the crash-box behavior, it is necessary to have a good approximation of the strain-rate sensitivity and strain hardening with temperature T and strain rate $\dot{\varepsilon}^p$. Of course, the temperature increases are local and will affect just a small part of the crash box where the collapse takes place. In this part of the crash box the plastic deformation level is close to 1 [15]. Several recent material models overcome this difficulty [7,16–19] but not many finite element commercial codes include these effects. The problem could be solved only by developing an algorithm to integrate the thermo-visco-plastic constitutive relation and implementing it in a user subroutine [20]. Such task has been done previously by the authors to solve different loading cases and to analyze dynamic instabilities, for example [12,16].

Having an accurate analytical description of the material behavior, it is necessary to apply this information to simulate numerically the behavior of a structure, in particular, to characterize the response of a crash box.

2. Experimental and numerical procedure used to characterize a crash test

In order to find the response of a structure in the form of a crash box several experimental setups may be used as it is shown in Fig. 6. In the first case, a mass is accelerated to an initial velocity V_0 with a hydro-pneumatic arrangement or by explosive driving. The roller impacts a structure fixed to the rigid wall made of steel or concrete. The second most popular setup is a drop tower where the mass M is released from the height h, which defines the initial impact velocity, $V_0 = \sqrt{2gh}$. In this arrangement the initial impact velocity V_0 is limited since it depends on the height of the drop tower. Thus, the first technique is used for relatively high impact velocities and the second for the intermediate range. In addition a direct impact of striker on a crash box supported by Hopkinson bar may be also used, for example [21], to analyze the response of a small crash box for the intermediate impact velocities.

Several kinds of specimen are currently used for crash tests, Fig. 7. Those specimens are with symmetric or asymmetric cross sections. The most popular is certainly the top-hat specimen, Fig. 7(a). Some variances can also be found, for example with injection of metallic or polymer foam into the structure [22–24]. In present case the top-hat geometry was chosen since this structure is generally used in automotive industry, Fig. 3(a).

The crash box is fixed to a rigid wall, Fig. 6(a), with a hydraulic system that assures a complete clamping of the structure during the test. Positioning of the specimen follows the sequence depicted in Fig. 8(a): it is inserted in a guide up to the contact with the wall, steps I and II, and then it is gripped by a mechanical or hydraulic device, step III, to ensure its stability during the test. This boundary condition is closely represented by restrictions in the displacements corresponding to case BC4 in the table 1 of Fig. 8. The boundary condition BC2 is similar to BC4 but introduces a stronger restriction to the displacements of surfaces S1 when the gripping device applies a higher force. In some cases a bad fixation may appear allowing some displacements of surfaces S1 or S2 that could be represented by boundary conditions BC1 or BC3 in Fig. 8. In the present work the four boundary conditions were considered. With this kind of boundary conditions (clamped surface), the displacement at the fixed side is zero. This causes that on that side the stress level is doubled, $2\sigma_I$. Of course, this happens due to the reflection of the incident elastic wave σ_I. This problem is analyzed in the following section of the paper. As reported in the literature, a crash box has commonly the maximum length $L_{max} \leqslant 1\,m$. Considering $L = 0.3\,m$ (current value of the crash-box length in this work), the first passage of the

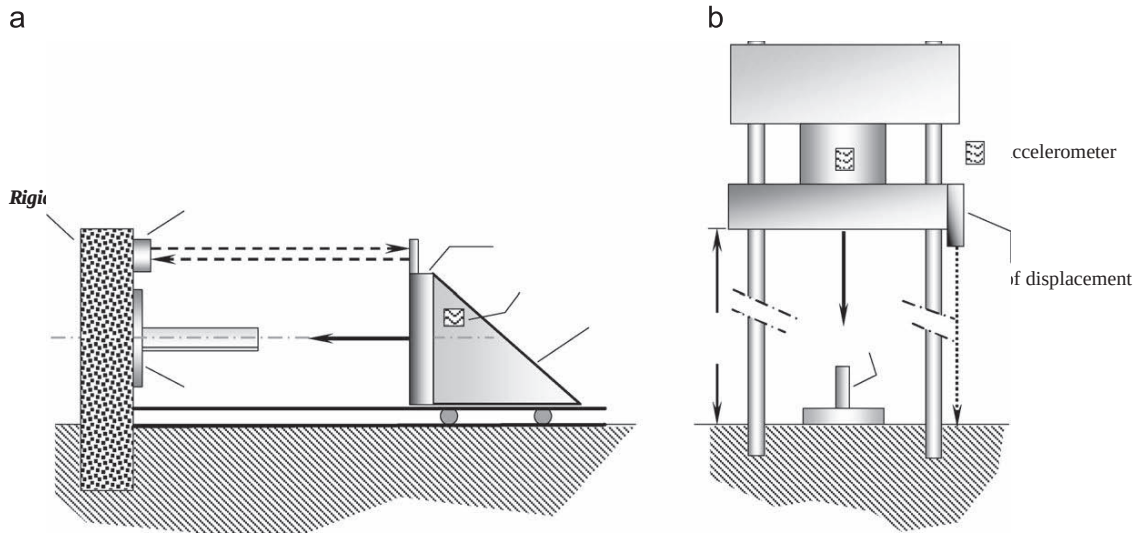

Fig. 6. Dynamic crash test setups: (a) catapult [43] and (b) drop tower [44].

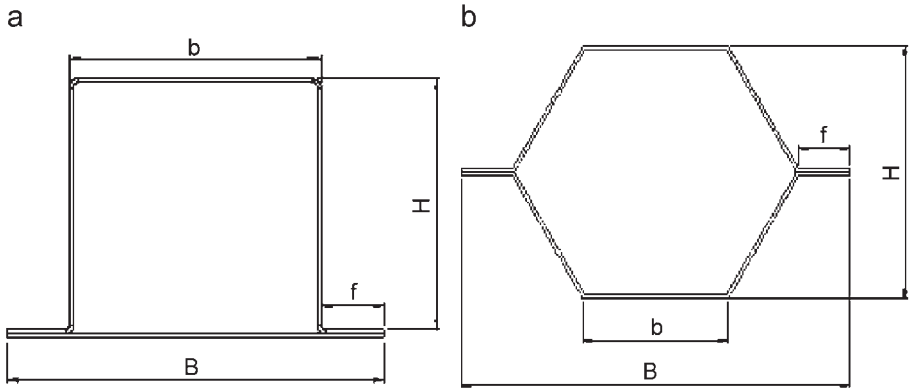

Fig. 7. Geometry currently used in crash experiment: (a) top hat specimen and (b) hexagonal specimen [37].

elastic wave is complete in $t_{\max}^{\text{elastic wave}} = 60\,\mu s$. This time interval is very short in comparison to the time corresponding to appearance of the first collapse. The external forces exerted on both sides of the specimen were determined in the first time on the support side and in the second time using the acceleration of the rigid plate on the impact side. Four triggers were introduced in the model on the impact side to get a repetitive folding mode on this part of the specimen. The symmetric trigger, Fig. 9(c), is obtained moving the first nodes of each elements in the thickness corresponding to one line of nodes as reported, Fig. 9(c) (symbol X and Y). Such trigger distribution is frequently used as reported in [25,26]. It is also observed that imperfection normally does not determine the collapse mode but accelerates the convergence during calculation [26].

To perform the numerical simulations, the finite element commercial code ABAQUS/Explicit [27] has been used. In the case analyzed a mass is launched with an initial impact velocity $V_0 = 16\,m/s$, Fig. 9(a). It was verified that the results of the simulations were the same when modeling the mass with solid elements and elastic behavior or as a rigid plate. Thus, the second case was chosen for simplicity. The adiabatic conditions of deformation have been assumed during all numerical calculations. The geometry of the crash box was discretized with 25812 8-node brick elements with reduced integration (C3D8R in ABAQUS notation) corresponding to 40312 nodes. Generally the minimum size element imposed by automotive industries recommendation is 5 mm [28,29]. In our case, a smaller size element has been chosen using a convergence method, comparing the force–time history and the collapse definition. When the force was stable using a smaller size the previous mesh was considered as optimal. To reduce the computation time two elements through the thickness were assumed. A convergence study has demonstrated that 3 or 5 elements give the same time history results. To have an optimal mesh, several quantities have been compared between all meshes, the force level, the collapse time and the number and shape of collapse folds. It was found comparing

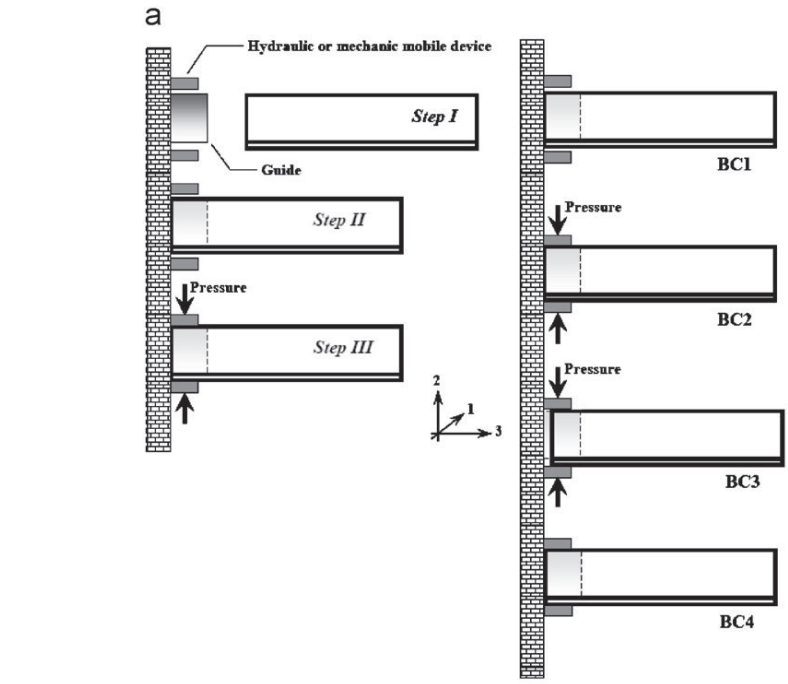

b

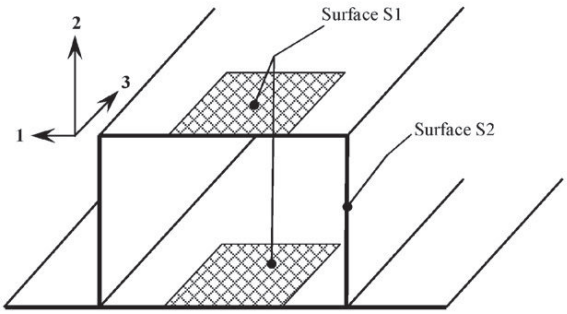

	S1 (Area)	S2 (Thickness Area)
BC1	without	$U_i = 0$
BC2	$U_i = 0$	$U_i = 0$
BC3	$U_i = 0$	without
BC4	$U_2 = 0$	$U_i = 0$

Fig. 8. Definition of the boundary conditions used during numerical simulations and effect of the boundary condition on the wave propagation.

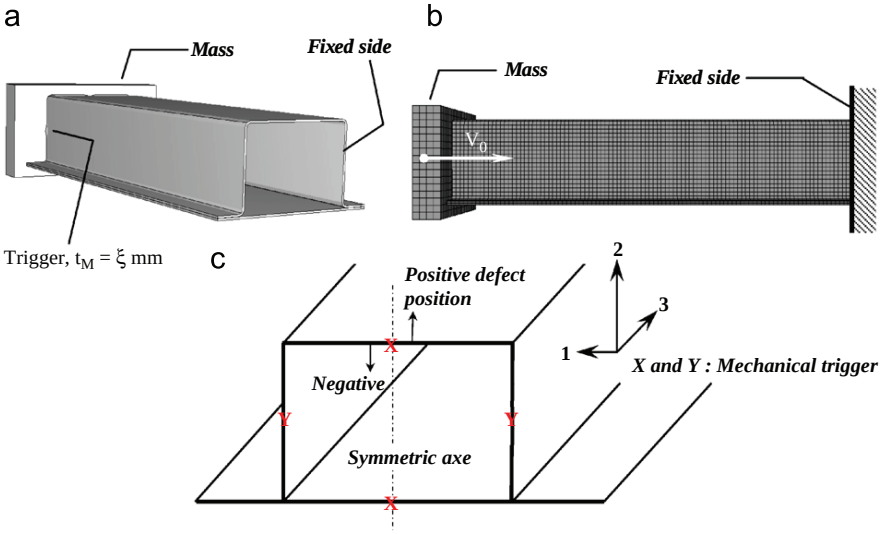

Fig. 9. (a) Definition of the crash box applied during experiment; (b) definition of 3D mesh assumed during numerical simulation and (c) trigger distribution with several configurations and symmetric distribution.

different simulations with more dense mesh that the results were the same. The spot weld points have been introduced in the present approach by using an option given by the code. According to industrial observations an interaction radius $\phi = 8$ mm with no damage was considered for the weld point. The behavior of spot welds is defined as rigid in the interaction zone. The friction coefficient $\mu = 0.1$ has been assumed via a contact algorithm. This algorithm allows simulation of the contact between the tube and the impacting mass and also the self-contact of sheets of the tube.

Having defined the structure and the boundary conditions, the process of collapse of the crash box using different constitutive models was analyzed. This is discussed in the next part of the paper. However, to demonstrate the effect of elastic wave propagation the perfectly plastic behavior has been introduced with different yield levels. This is the first approximation to the crash-box simulation. It is also possible to describe more precisely the thermo-visco-plastic behavior of material studied using a VUMAT (User Subroutine) procedure in ABAQUS. Such simulations have been realized previously by the authors to study the effect of constitutive relation for different dynamic applications. In this paper a particular attention is given on the coupling of elastic wave propagation and plasticity. For this reason the behavior is defined as perfectly plastic to have a good understanding of the coupling and to dissociate all other effects as the strain-rate sensitivity, temperature sensitivity and strain hardening. Previous works of other authors demonstrated that the problems of dynamic buckling are strongly dependent on inertia and strain-rate effects [2,30].

3. Effect of plasticity on response of crash box

3.1. Elementary elastic wave propagation theory

In this part a brief introduction on the elastic wave propagation in slender rods is presented. The longitudinal elastic waves are developed by an impact on the end of rod. The second end can be fixed or being free. This will illustrate the problem discussed later in this paper concerning the competition between the local plastic deformation and the process of elastic wave reflection from the fixed end of the rod. In order to present the problem a simple case is considered using 1D approach. Fig. 10 shows the situation. During an impact on a bar with velocity V_0, an incident elastic wave $\sigma_I(t)$ is generated. This wave propagates along the bar with elastic wave speed C_0 which is related to the Young's modulus E and the density of the bar material ρ. For steels this celerity is $C_0 = \sqrt{E/\rho} \approx 5000\,\mathrm{m/s}$. The time interval needed to reach the opposite side of the bar is relatively short. Assuming the typical lengths of crash box currently reported in the literature, varying within the limits $300 \leqslant L_0 \leqslant 500$ mm [1], the travel time varies from $0.06 \leqslant t_L \leqslant 0.1$ ms.

The 1D problem of elastic wave propagation is formulated via the local force equilibrium of the bar with a constant cross-sectional area. The wave propagation is defined by the following differential equation:

$$-\frac{\partial}{\partial x}\left(AE\frac{\partial u}{\partial x}\right) + \rho A\frac{\partial^2 u}{\partial t^2} = 0, \quad 0 \leqslant x \leqslant L, \tag{1}$$

where A is the cross-sectional area and E is the Young's modulus. The solution of Eq. (1) is given in the form of

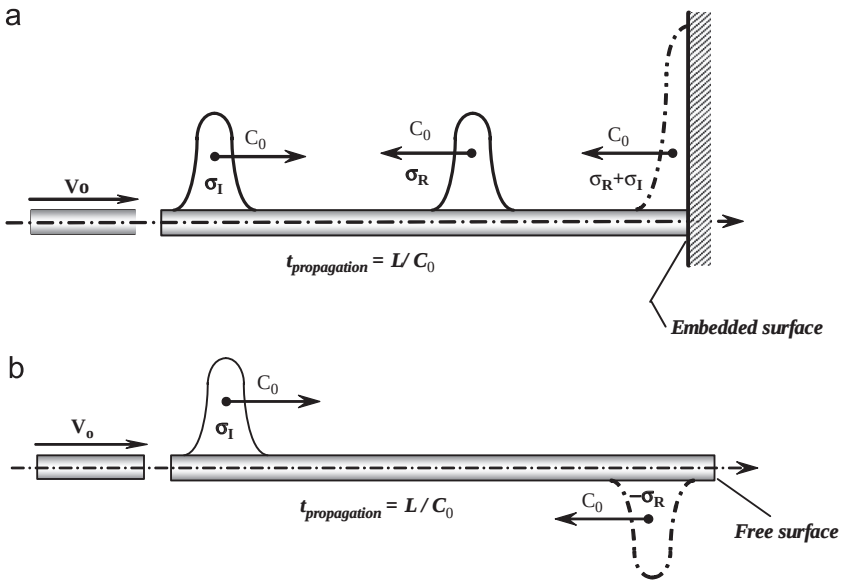

Fig. 10. Schematic representation of elastic wave propagation along elastic bar: (a) reflection of longitudinal wave from the fixed end and (b) reflection from the free end.

Lagrange displacement $u(x, t)$ [31], by

$$u(x,t) = U_I(x,t) + U_R(x,t) = f(x - C_0 t) + g(x + C_0 t), \tag{2}$$

where f is a function which defines the wave propagation in the positive direction, $x>0$, and g is the same for the negative direction, $x<0$. For the case of rigid attachment shown in Fig. 10(a) the boundary conditions impose displacement equal to zero at $x = L$ and the stress level is the sum of the incident wave σ_I and the reflected wave σ_R. Thus,

$$\begin{cases} V(L,t) = -C_0(f'(L - C_0 t) - g'(L + C_0 t)) = 0, \\ s(L,t) = s_I(L,t) + s_R(L,t). \end{cases} \tag{3}$$

Using the Hooke's law, it is possible to relate the stress with the elastic strain level for the incident and reflected wave

$$\begin{cases} \sigma_I(x,t) = E\varepsilon_I(x,t) = E\dfrac{\partial f}{\partial x}, \\ \sigma_R(x,t) = E\varepsilon_R(x,t) = E\dfrac{\partial g}{\partial x}. \end{cases} \tag{4}$$

The boundary condition at $x = L$ (velocity is equal zero, Eq. (3)) allows to write:

$$f'(L,t) = g'(L,t). \tag{5}$$

Taking into account Eq. (5), the stress level of the reflected wave can be found as a function of the incident elastic wave

$$\begin{cases} \sigma(L,t) = \sigma_I(t) + \sigma_R(t), \\ \sigma(L,t) = E\left(\dfrac{\partial f}{\partial x} + \dfrac{\partial g}{\partial x}\right) = 2E\dfrac{\partial f}{\partial x}, \\ \sigma(L,t) = 2\sigma_I(L,t). \end{cases} \tag{6}$$

In conclusion, the stress at the fixed end is twice of the incident stress σ_I. This effect is directly related to the position of the collapse site observed during numerical simulations of a crash box. It is discussed in the following part of the paper.

Using the similar approach it is relatively easy to demonstrate that for the free boundary condition at $x = L$, $\sigma = 0$ and the displacement is doubled, Fig. 10(b) [31]. At the same time the reflected wave changes from compression to tension. Such situation is also shown in Fig. 10(b).

In order to demonstrate the elastic wave propagation through the crash box, the first calculation has been performed for pure elasticity where the behavior is defined by the Young's modulus E and the Poisson's ratio ν, Fig. 11. The initial impact velocity was assumed to be $V_0 = 16\,\text{m/s}$, which corresponds to the incident stress amplitude $\sigma_I = \rho C_0 V_0 = 624\,\text{MPa}$. The boundary conditions are shown in Fig. 11(a). After the first reflection at $x = L$ the stress level is doubled $\sigma_R = 1248\,\text{MPa}$, Fig. 11(b). This is in agreement with Eq. (6).

3.2. Perfectly plastic behavior

3.2.1. Effect of the yield stress on the collapse process

To analyze the influence of the value of the yield stress on the process of the crash-box collapse, the perfectly plastic behavior ($\sigma_y = \text{const.}$) has been assumed, Fig. 12(a). The real value of the yield stress for ES mild steel is $\sigma_y = 180\,\text{MPa}$, but several yield levels have been assumed to analyze the effect of this value on the collapse side. The level of plastic deformation depends on the yield stress in relation to the wave stress, $\sigma_I = \sigma_{shock} = \rho C_0 V_0$. In *case I*, Fig. 12(b), the yield stress assumed is lower than the stress amplitude (σ_{shock}) and plastic deformation occurs close to

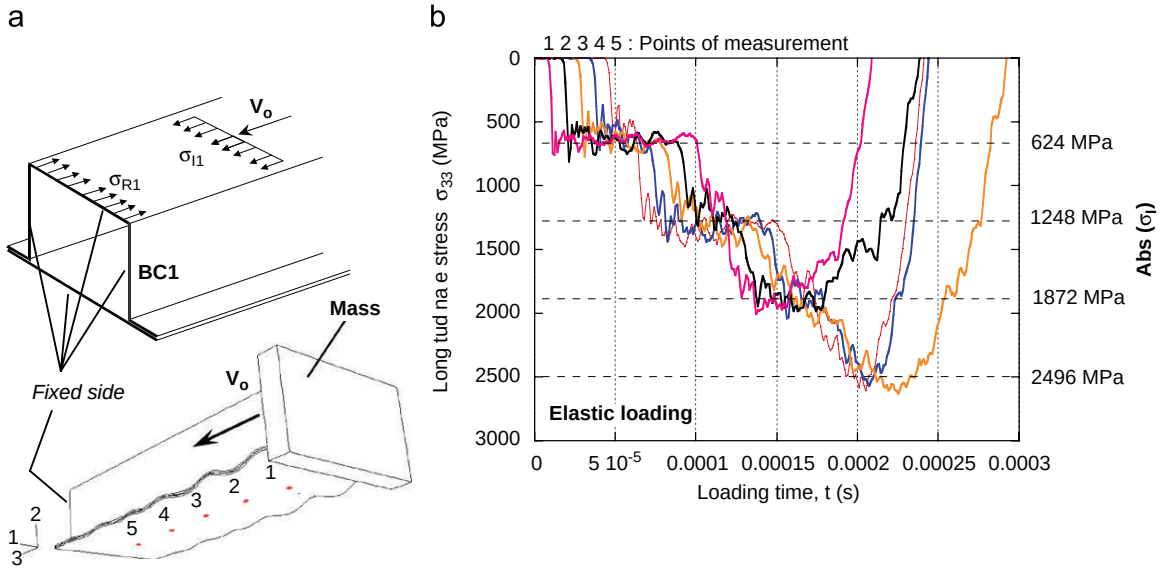

Fig. 11. (a) Definition of the boundary condition and point of analysis and (b) effect of the fixed end on the elastic wave propagation in crash box.

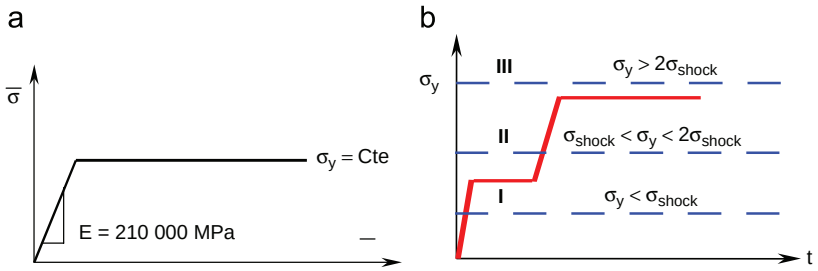

Fig. 12. (a) Behavior assumed during numerical simulations using elastic perfectly plastic material and (b) schematic representation of the process of elastic wave reflection, case I double stress level is possible ($\sigma_I < \sigma_y$), case II stress level increase is possible at the clamped side ($2\sigma_I > \sigma_y$).

the impact side. On the contrary, in *case II*, if the yield stress is between $\sigma_{shock} \leqslant \sigma_y \leqslant 2\sigma_{shock}$, no plastic deformation may occur on the impact side but on the opposite side, due to the effect of double stress (stress reflection). Concerning *case III*, the yield stress is assumed very high, no plastic deformation may appear when the incident elastic wave reaches the opposite side. In the present analysis only *cases I* and *II* are studied, they correspond to real configuration observed during experiment.

The numerical results corresponding to BC1 with the friction coefficient $\mu = 0.1$ and with the initial mesh defect $t_M = 3$ mm are shown in Fig. 13. It is observed that the collapse site is directly affected by the plastic stress level imposed σ in relation to the yield stress σ_y. For a low yield stress σ_y an important plastic deformation is observed on the impact side inducing an instantaneous collapse closer to this side. This collapse reduces the stress level propagating in the crash box and prevents collapsing on the opposite side. This observation is true provided the yield stress is lower than $\sigma_y \leqslant 400$ MPa. Now, if the yield stress is assumed higher, $\sigma_y > 400$ MPa, the plastic deformation is reduced, no collapse takes place on the impact side. In this case, a superposition of the incident wave $\sigma_I(t)$ and reflected wave $\sigma_R(t)$ induces an increase of axial stress on the clamped side, *case II*, Fig. 12(b). The result is a collapse close to the support side.

For $\sigma_y = 400$ MPa, the plastic deformation develops closer to the impact side and at the same time, due to elastic wave propagation, the plastic deformation appears also on the opposite side. It occurs due to an increase of stress level (phenomenon of superposition of incident $\sigma_I(t)$ and reflected $\sigma_R(t)$ waves on the clamped side). This is the main reason why two collapse sites are observed. Such phenomenon is also visible for the same reason for $\sigma_y = 450$ MPa.

The collapse phenomenon is controlled by the force–time evolution as shown in Fig. 14, for three cases where the yield stress varies in the limits $150 \leqslant \sigma_y \leqslant 600$ MPa. The axial stress plotted corresponds to the nominal stress obtained by division of the input (impacted side) and output (support side) forces by the area of the initial cross sectional of the crash box. Depending on the yield stress imposed, it is observed that the output force oscillates around the input force. Time $t = 0$ is the instant of impact and $t \approx 60$ μs is the characteristic time for elastic wave to reach the opposite side. Therefore, these oscillations are due to elastic wave propagation and they are previous to the development of the different wrinkles on the tube. For $\sigma_y \approx 150$ MPa the collapse appears on the impact side controlling the level of stress in the crash box. Therefore the output force oscillates around the input force with period equal to elastic wave round trip time (Fig. 14(a)). The opposite effect is observed for $\sigma_y \approx 600$ MPa (Fig. 14(c)). This occurs due to the wave propagation phenomenon described previously. For $\sigma_y \approx 400$ MPa, due to simultaneous collapse on each side, no oscillations appear (Fig. 14(b)). In this case, the stress oscillations are avoided on input and output sides since plastic deformation is taking place on both of them. According to plots, Fig. 14, the first local collapse event induces a fast increase of the axial deformation and a decrease of the axial force level for example if the first collapse take place on the impact side, Fig. 14(a). This information is propagated in the axial direction and prevents any other collapses along the structure (as long as two folds are not in contact). Finally, all possible cases of collapse processes may be summarized by Fig. 15.

In the first case of diagram, Fig. 15, as long as the yield stress is lower than the elastic shock level ($\sigma_y^{static} < \sigma_I^{Elastic}$), an instantaneous plastic deformation appears on the impact side inducing a collapse to the impact side. Whereas incident wave propagates along the crash box, the plastic strain level is increasing with a low strain rate. If the quasi-static yield stress is much lower than the elastic shock level, a fast buckling appears on the impact side before the propagation time corresponding to $t = L/C_0$. The buckling leads to a decrease of the axial stress level and prevents any other collapses. The second case ($\sigma_y^{static} \approx \sigma_I^{Elastic}$) corresponds to the transition case: if the quasi-static yield stress is quite close to the elastic shock level, the plastic strain increases slowly on the impact side. Thus, the buckling on impact side is delayed and do not prevent a collapse process on the opposite side when the incident wave reaches the opposite side. It is the reason why a double collapse appears in this case. The third case, Fig. 15, corresponds to a higher quasi-static yield stress in comparison with the elastic shock level ($\sigma_y^{static} > \sigma_I^{Elastic}$). In this case, no buckling is triggered on the impact side

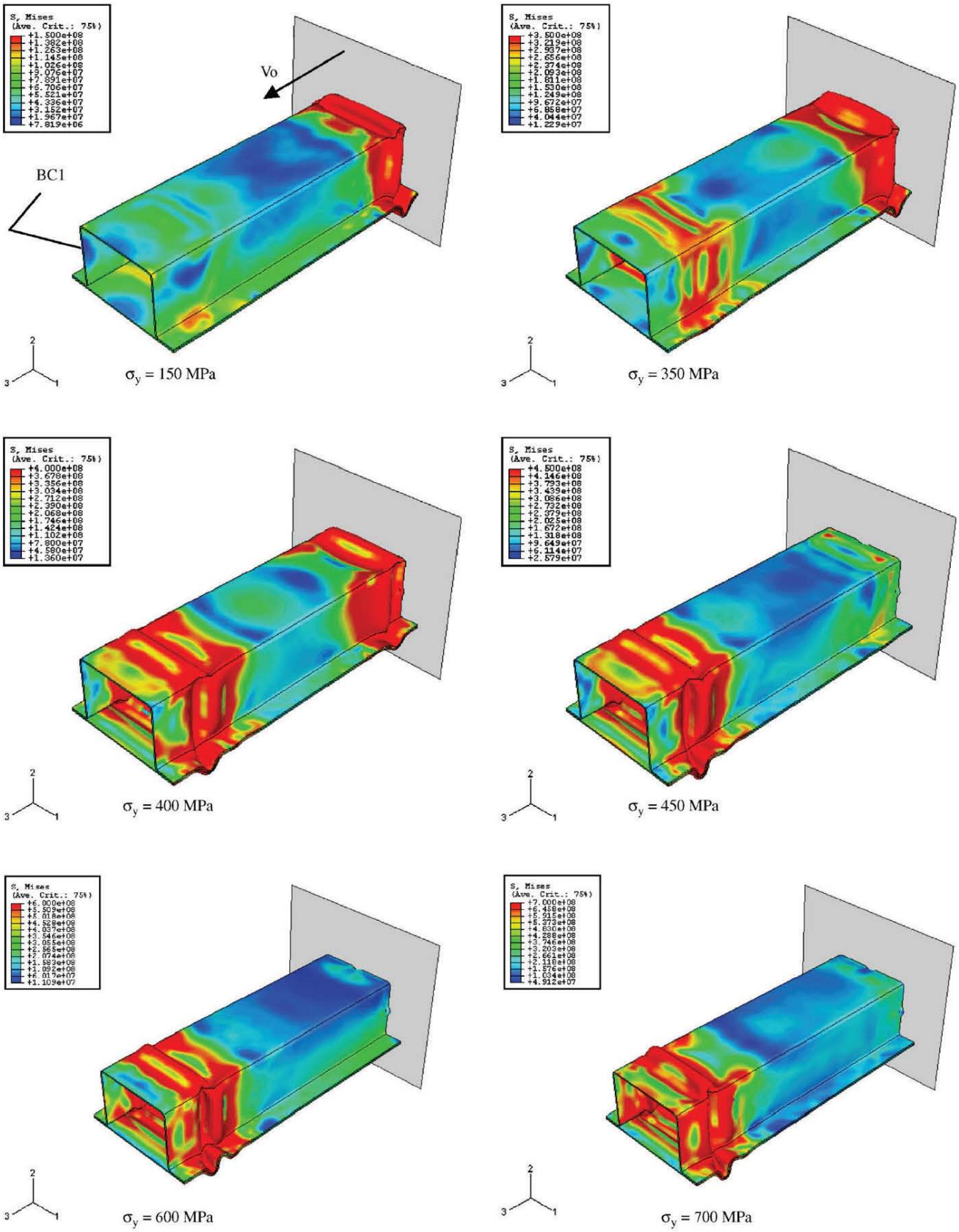

Fig. 13. Numerical simulations using a perfectly plastic behavior and boundary conditions type BC1 for $V_0 = 16\,\text{m/s}$, $\mu = 0.1$ and $t_M = 3\,\text{mm}$.

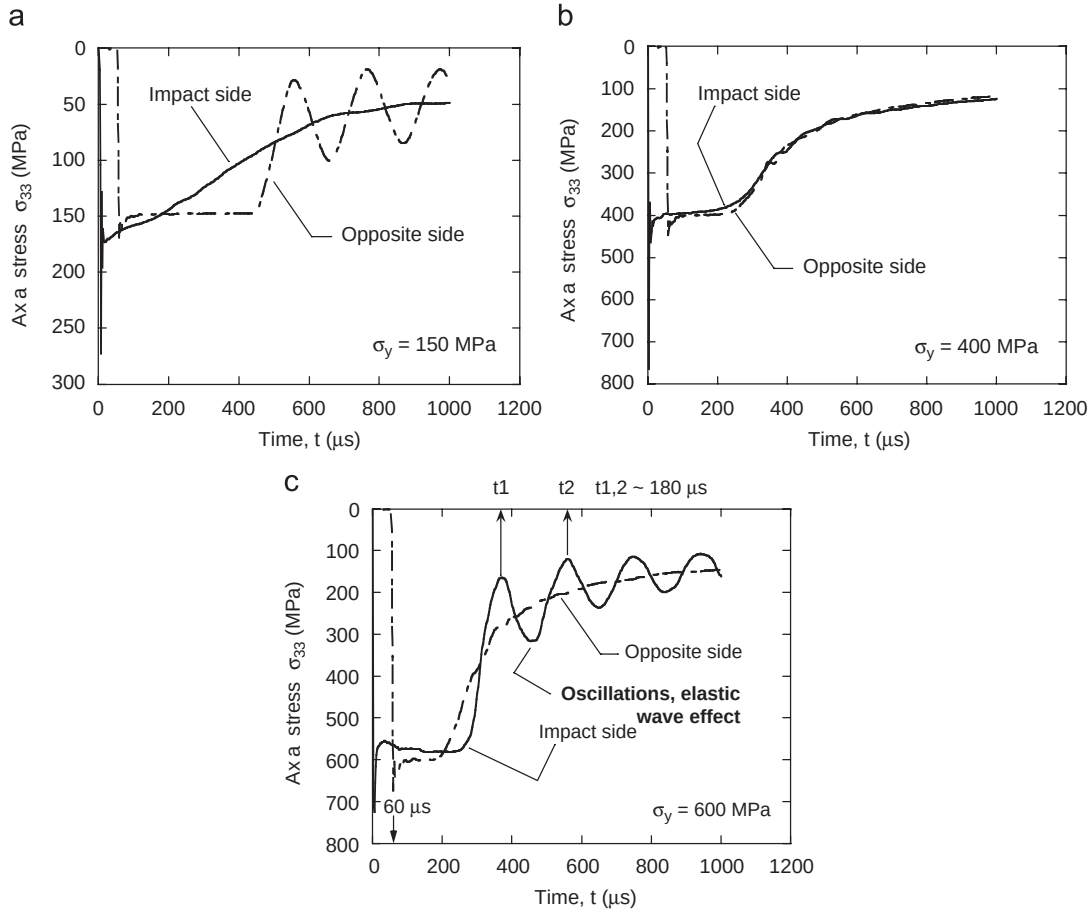

Fig. 14. Comparison between impact side force and opposite force for BC1, $V_0 = 16\,\text{m/s}$, $\mu = 0.1$ and $t = 3\,\text{mm}$.

during the first round trip time. Thus, the incident wave propagates up to the embedded side. The reflected wave leads to a twice of axial stress level on the opposite side ($2\sigma_{\text{I}}^{\text{Elastic}}$) and must be compared with the dynamic yield stress of the crash box. Three cases are once again possible. The first one ($\sigma_{\text{y}}^{\text{Dynamic}} < 2\sigma_{\text{I}}^{\text{Elastic}}$) induces a fast increase of the plastic strain level on the opposite side leading to an instantaneous collapse on this side. Concerning the second case ($\sigma_{\text{y}}^{\text{Dynamic}} \approx 2\sigma_{\text{I}}^{\text{Elastic}}$), the plastic strain develops slowly on the opposite side. Therefore, the delayed buckling does not prevent a collapse on the impact side after the round trip time ($t > 2L/C_0$). Finally, in the case of a dynamic yield stress higher than the twice of axial stress level $\sigma_{\text{y}}^{\text{Dynamic}} > 2\sigma_{\text{I}}^{\text{Elastic}}$, no buckling is possible on the opposite side at time $t = L/C_0$. Therefore, as shown in Fig. 11, the reflected wave which reaches the impact side after one wave travel and due to the contact between the crash box and the mass reacts as the embedded side. In this case, the cumulated plastic strain on the impact side produces a fast collapse on that side.

In conclusion, the problem of crushing is governed both by plasticity and by elastic wave propagation. A process of collapse may appear on the opposite side of impact due to the embedded boundary condition on this side coupled with the phenomenon of elastic wave reflexion. Moreover, as it will be discussed later, an effect of strain-rate sensitivity is observed due to the difference of loading rates between the impact side and the opposite side requiring a correct definition of the thermo-visco-plastic behavior, $\sigma(\varepsilon^{\text{p}}, \dot{\varepsilon}^{\text{p}}, T)$, of the steel used for the crash box. The coupling of elastic wave propagation and thermo-visco-plastic behavior is discussed later as well as the influence of the boundary conditions (type of embedding condition, size of trigger, friction coefficient between the mass and the crash box).

4. Effect of boundary conditions and geometric defects on the response of the crash box

4.1. Effect of boundary conditions

In the previous part, the analyses have been limited to the boundary conditions BC1 (opposite side completely clamped). Now, the other three boundary conditions are considered to study their effect on the localization of plastic deformation, also assuming the perfectly plastic behavior for the crash-box material (Fig. 16). Two extreme cases are assumed concerning the yield stress, that is $\sigma_{\text{y}} = 150$ and

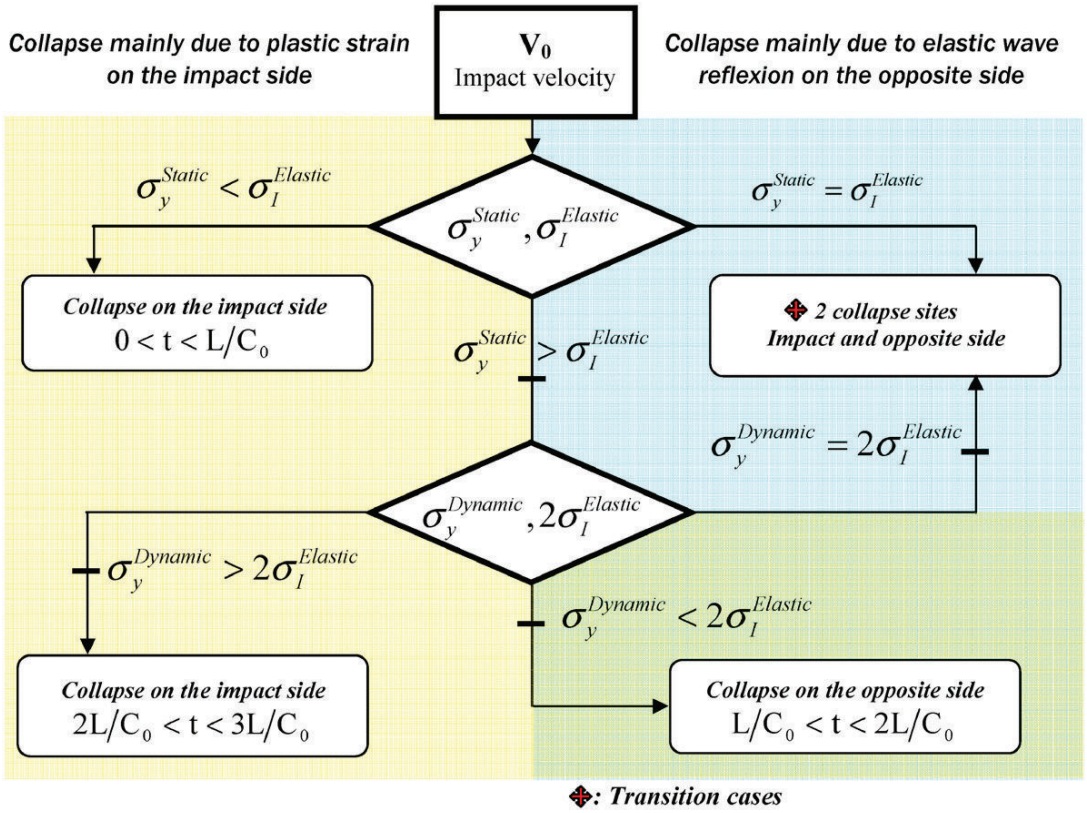

Fig. 15. Schematic representation of different collapse processes that may occur depending of the yield stress level of the crash box.

600 MPa. Since BC1, BC2 and BC4 conditions impede the axial displacement at the support side, the double stress effect takes place, producing collapse on this side for high values of σ_y. When imposing BC3 boundary conditions, a local stress concentration appear close to the gripping surface (S1 in Fig. 8) and local folding develops on this zone even for the low value of yield stress. The boundary conditions must be defined precisely in the numerical model to obtain an agreement with experimental tests in terms of number and localization of collapse lobes.

Therefore the first conclusion is that the collapse process of crash box depends on the plastic behavior of material, but at the same time is also governed by elastic wave propagation.

4.2. Effect of friction coefficient

The friction coefficient μ between the mass and the box has also an important role on the process of collapse. When $\mu = 0$ sliding at the contact surface is favored and transverse displacements of the edge of the tube takes place easily. This facilitates the collapse on the impacted side. In fact, with $\sigma_y = 600$ MPa folding may appear on this side (Fig. 17(a)) if no friction is included in the contact model, whereas collapse occurs on the opposite side for a value of $\mu = 0.1$, Fig. 17(b). Thus, the collapse site also depends on the level of friction.

In agreement with previous explanations, Fig. 14, the oscillating force corresponds to the no collapse side, Fig. 17(a) and (b). The additional analysis on the effect of geometric trigger has been performed since the trigger is frequently assumed in numerical simulations as an initiator of collapse or instability.

4.3. Effect of trigger size

In order to get a repetitive folding mode, geometric defects are commonly produced on the tube both in experimental and numerical studies. The size of these defects, called triggers, may also change the position of the collapse as can be seen in the following results. Different trigger sizes are analyzed varying from $1 \leqslant t_M \leqslant 5$ mm with the same trigger arrangement as discussed previously. The perfectly plastic behavior is considered with the yield stress $\sigma_y = 400$ MPa. This stress level as discussed previously, Fig. 13, corresponds to the transition between collapse on the impact and on the opposite sides. With the trigger size $t_M = 1$ mm the collapse takes place on the opposite side, Fig. 18(a), whereas for $t_M = 5$ mm the collapse is observed on the impact side, Fig. 18(b). Therefore, the transition case ($\sigma_y = 400$ MPa) may be influenced by the trigger size. But this parameter does not influence the results of collapse for higher or lower yield stress than $\sigma_y = 400$ MPa.

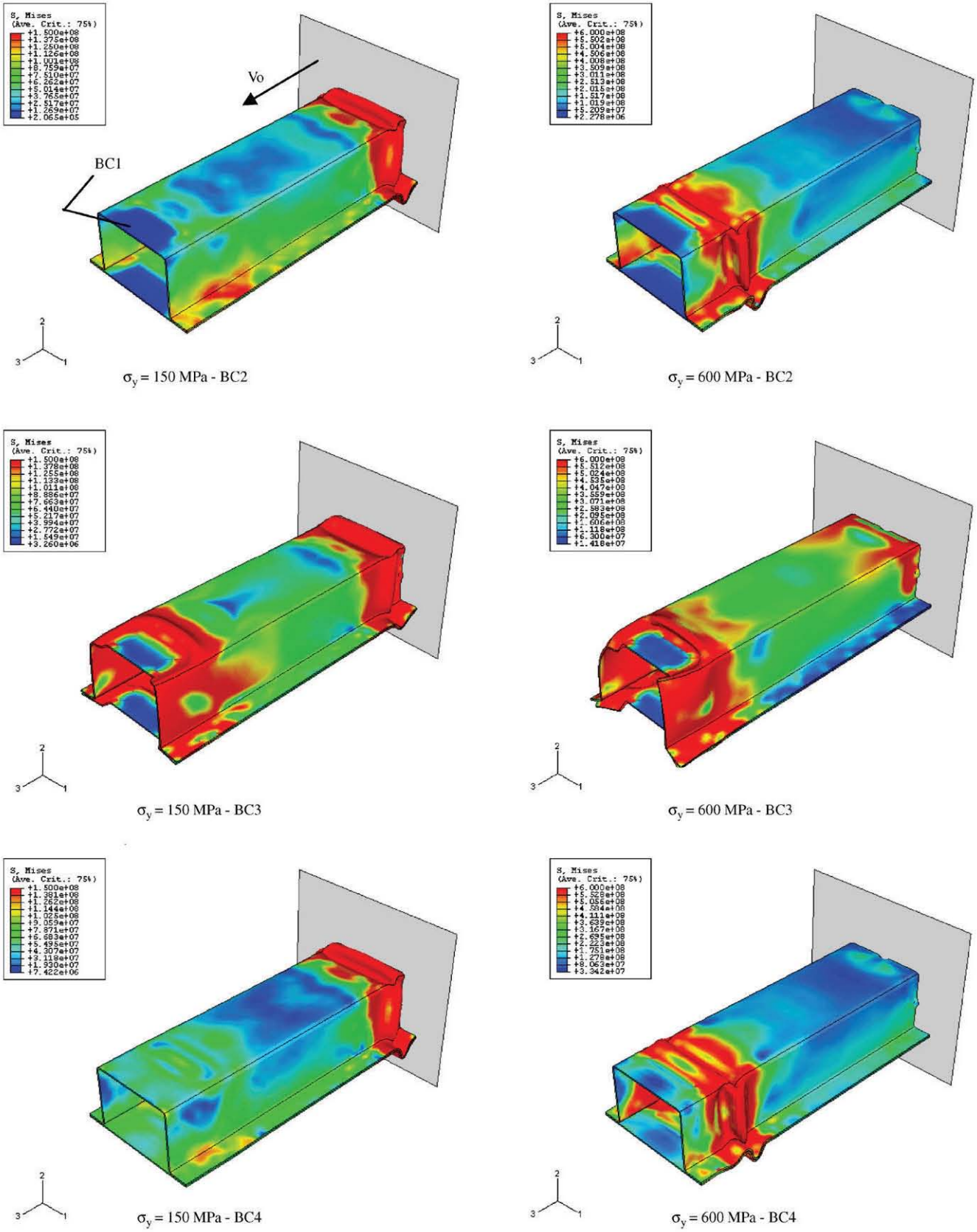

Fig. 16. Numerical simulations using perfectly plastic behavior and different boundary conditions for $V_0 = 16\,\text{m/s}$, $\mu = 0.1$ and $t_M = 3\,\text{mm}$.

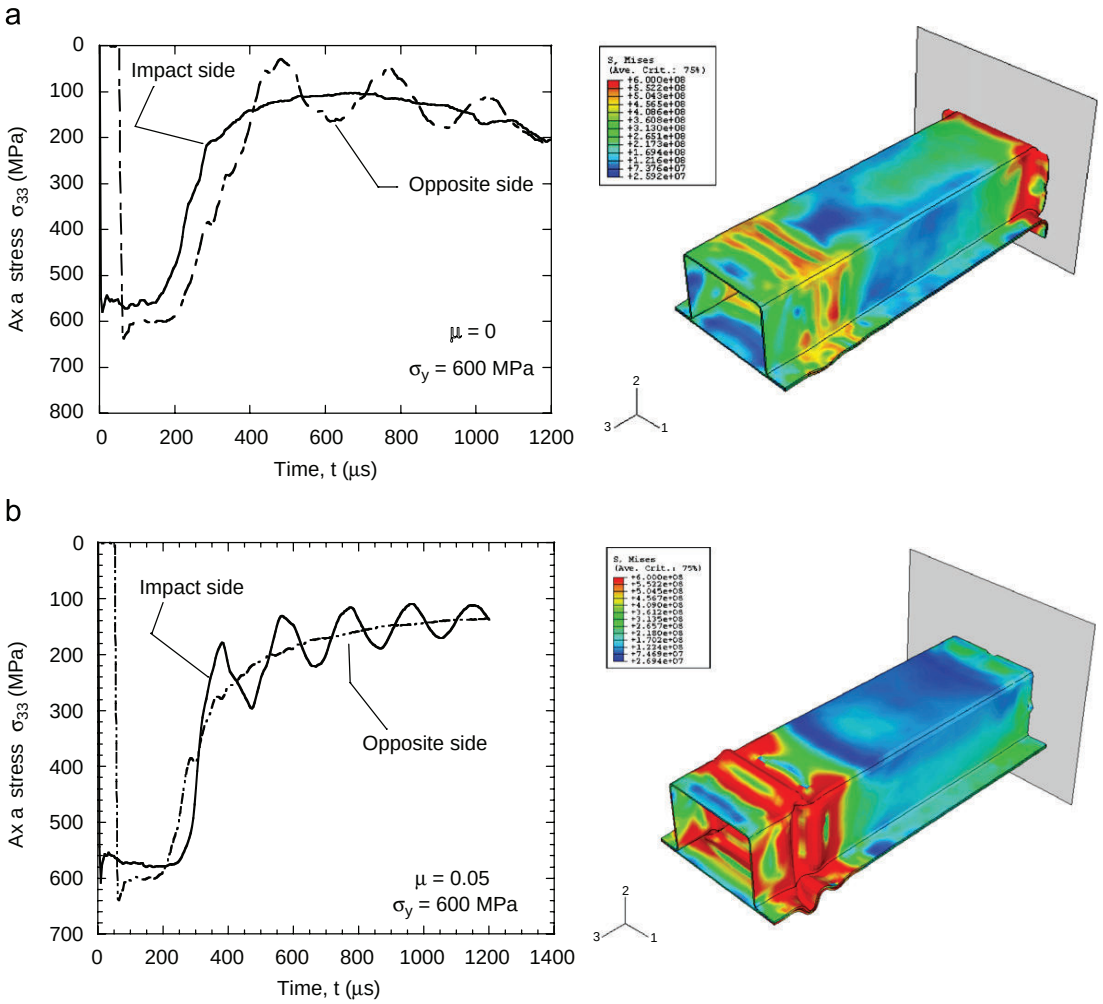

Fig. 17. Effect of friction coefficient on the collapse site for BC1, $V_0 = 16\,\text{m/s}$, $t_M = 3\,\text{mm}$: (a) $\mu = 0$ and (b) $\mu = 0.05$.

In order to complete these analyses and to study the contribution of mechanical properties, it is interesting to demonstrate the effect of strain-rate sensitivity. Indeed, during the first impact, the local strain rate of $\dot{\varepsilon}^p \approx 10^3\,s^{-1}$ is observed. The strain-rate sensitivity induces an increase of the stress level. Thus, the strain-rate sensitivity is the unique effect allowing inhibition of the double stress level due to the process of elastic wave superposition that appears on the side opposite to impact. The goal is to obtain a plastic stress level σ on the impact side much higher due to strain-rate sensitivity in comparison with the yield stress σ_y observed in quasi-static loading. In order to perform this analysis a simple constitutive relation with the constant strain-rate sensitivity $C = \partial\sigma/\partial \ln \dot{\varepsilon}$ is used.

5. Thermo-visco-plastic behavior with Johnson–Cook model and linear strain-rate sensitivity

To extend the analysis of the effect of the mechanical properties on the collapse site, new simulations were performed taking the parameters of different steels, Fig. 19(a). In the definition of the hardening of these materials, strain-rate sensitivity should play an important role: the average strain rate observed during a crash test is around $200\,s^{-1}$, but instantaneous values of this variable cover a large range, from quasi-static conditions, $\dot{\varepsilon}^p = 10^{-3}\,s^{-1}$, to large values above the strain-rate transition observed for mild steel $\dot{\varepsilon}^p = 10^3\,s^{-1}$, Fig. 4(a). As discussed previously, it is observed that hardening coefficient has also an important effect as it is reported in [32,33] changing the plastic wave speed $C_p = \partial\sigma/\partial\varepsilon^p$, Eq. (7b), Fig. 19(b), during first impact time. This effect is relatively reduced, Fig. 19(c), in comparison with the strain-rate sensitivity or the B parameter, Eq. (7a), Fig. 19(e). Thus, in this study a particular attention is given on the strain-rate sensitivity parameter since strain-rate sensitivity can increase instantaneously the yield stress of the material and the flow stress, Fig. 19(d). This effect modifies the collapse site in the crash tube. Thus, in the second part of this paper, the same analysis has been performed using a thermo-visco-plastic model, assuming relatively low and

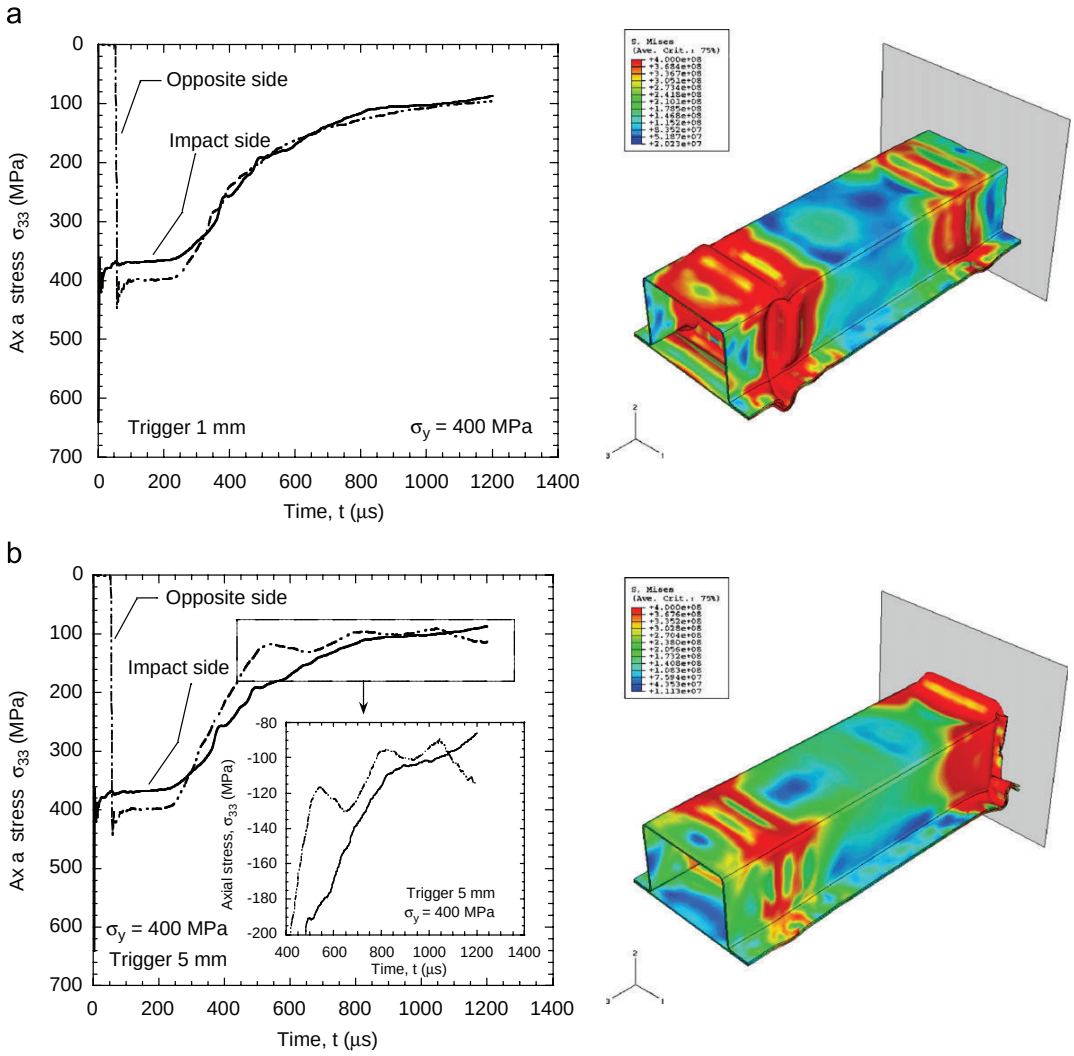

Fig. 18. Numerical simulations using perfectly plastic behavior and boundary conditions BC1 for $V_0 = 16\,\mathrm{m/s}$, $\mu = 0.1$ and $\sigma_y = 400\,\mathrm{MPa}$.

constant strain-rate sensitivity C, Eq. (7a). The constitutive relation used is that introduced by Johnson Cook [34]. It allows a correct approximation of strain-rate sensitivity of mild steels in quasi-static range of deformation, typically: $10^{-4} \leqslant \dot{\varepsilon}^{p} \leqslant 10^{2}\,s^{-1}$, Fig. 4(a). This constitutive relation is frequently applied in commercial FE codes used by industries. For the simulations the ABAQUS/Explicit code has been used in the commercial version. The explicit formulation of the Johnson Cook relation is given by

$$\sigma \quad (A + B(\varepsilon^{p})^{n})\left(1 + C \ln\left(\frac{\dot{\varepsilon}^{p}}{\dot{\varepsilon}_0}\right)\right) \times \left(1 - \left(\frac{T - T_{\mathrm{room}}}{T_{\mathrm{melting}} - T_{\mathrm{room}}}\right)^{m}\right), \tag{7a}$$

$$C_{p}\big|_{T_{\mathrm{room}}} \quad \sqrt{\frac{(Bn(\varepsilon^{p})^{n-1})(1 + C \ln(\dot{\varepsilon}^{p}/\dot{\varepsilon}_0))}{\rho}}. \tag{7b}$$

The constants for the steels studied are given in Table 1. The rate sensitivity C for mild steel ES assumed as C 0.0362 yields a very low stress increase versus strain rate, Fig. 19(a). The effect of strain rate on the flow stress is not well defined for strain rates higher than $\dot{\varepsilon} > 10\,s^{-1}$, Fig. 4(a). But the strain-rate range observed during crash tests is in between quasi-static loading to $\dot{\varepsilon}^{p} \approx 200\,s^{-1}$ on average. Therefore the JC constitutive equation with a constant value of C will not be predictive at relatively high strain rates. This is due to the fact of non-linear strain-rate sensitivity showed by many steels, Fig. 4(a). In order to define correctly the material behavior for all range of strain rates from quasi-static to dynamic loading, a suggested solution is to assume two rate sensitivities depending on the strain rate range, Fig. 4(a). Nevertheless, this is not possible in commercial finite element codes such as ABAQUS/Explicit. As the second step in this analysis, the effect of strain rate has been considered applying the JC

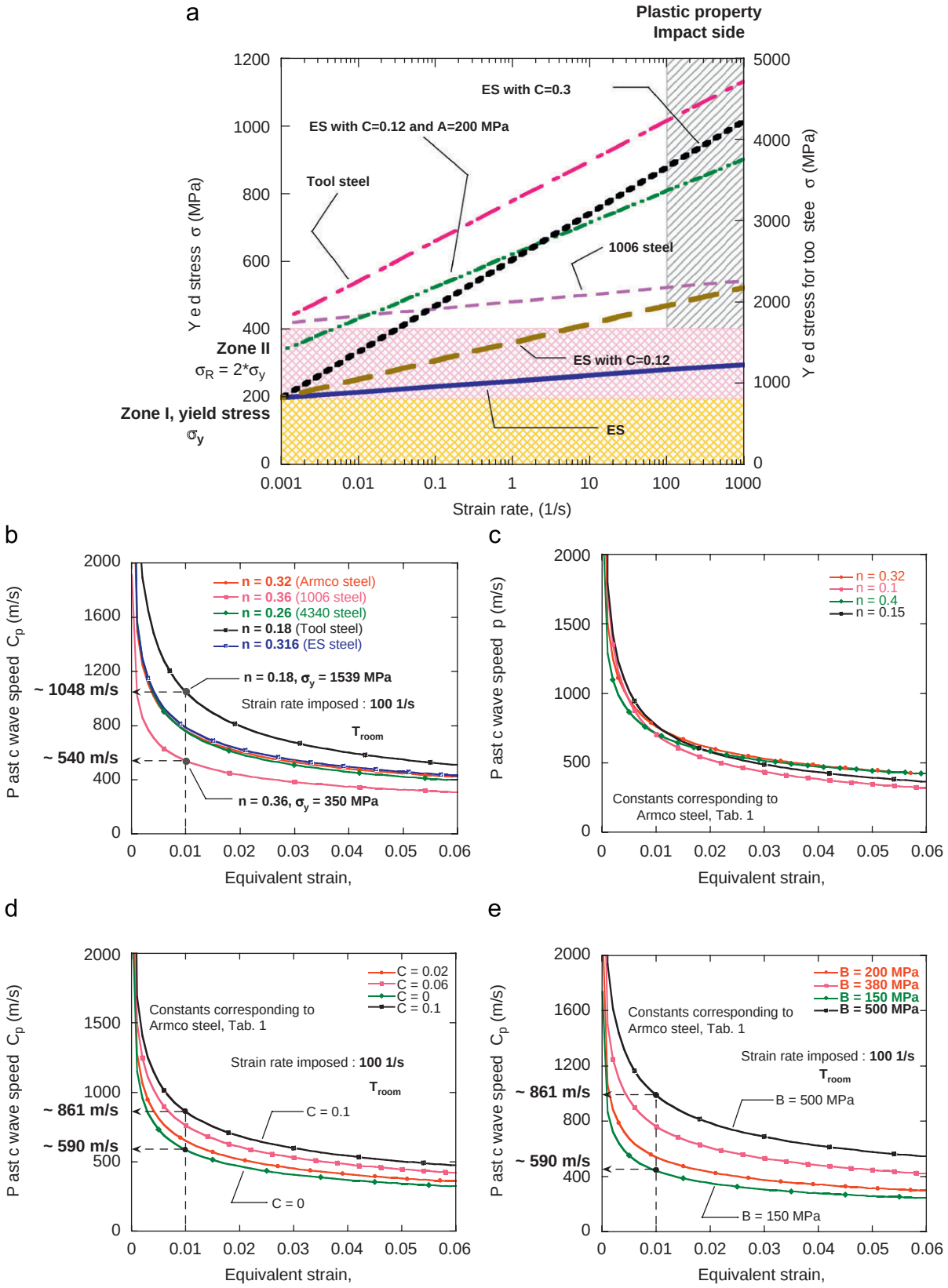

Fig. 19. (a) Strain rate sensitivities applied in CL constitutive relation for different steels [34]; (b) estimation of plastic wave speed depending of different hardening coefficient values; (c) effect of the hardening coefficient values for an imposed yield stress; (d) effect of the strain rate sensitivity on the plastic wave speed; (e) effect of *B* parameter on the plastic wave speed using JC model.

Table 1
Constants in JC constitutive relation for different steels [34]

Constants	Armco steel	1006 steel	4340 steel	Tool steel	ES steel
A (MPa)	175	350	792	1539	57.27
B (MPa)	380	275	510	477	479.93
n (1)	0.32	0.36	0.26	0.18	0.316
C (1)	0.060	0.022	0.014	0.12	0.0362
m (1)	0.55	1	1.03	1	0.28

constitutive equation corresponding to different materials, Table 1.

The strain rates sensitivities represented by different slopes are shown in Fig. 19. This figure provides the information needed to compare the yield stress corresponding to dynamic conditions, $\dot{\varepsilon}^{p} = 10^{3}\,s^{-1}$, with the stress level σ_I induced by the impact and their respective multiples due to successive reflections of the elastic wave.

Values of the rate sensitivities provide direct information concerning the competition between the stress value on the support side due to the process of elastic wave reflection and the intensity of the plastic stress level σ reached at $\dot{\varepsilon}^{p} = 10^{3}\,s^{-1}$ on the impact side. In fact during the first instants of impact the local strain rate is $\dot{\varepsilon}^{p} = 10^{3}\,s^{-1}$ and decreases to an average value of $\dot{\varepsilon}^{p}_{average} = 10^{2}\,s^{-1}$. Some artificial strain-rate sensitivities have also been considered concerning mild steel ES with $0.12 \leqslant C \leqslant 0.3$ and the same yield stress for quasi-static loading at $\dot{\varepsilon}^{p} = 10^{-3}\,s^{-1}$, Fig. 19.

The numerical results are shown in Fig. 20. It is observed that the first collapse takes place in different sides depending of the thermo-visco-plastic properties and strain-rate sensitivity. In the case of mild steel ES with $C = 0.0362$, collapse appears at both sides of the box, Fig. 20(c). Therefore, this corresponds to the transition case, as discussed previously with perfectly plastic material behavior. If the strain-rate sensitivity increases ($C = 0.12$ or $C = 0.30$) the collapse takes place at the impacted side, Fig. 20(d) and e. In these cases the dynamic yield stress is very high and it is difficult to reach the yield stress both on the impact side and on the clamped side. The plastic deformation can only appear after two passages of elastic wave. When the reflected elastic wave reaches the impacted side after $t = 2L/C_o$ the stress is high enough to deform plastically the material.

Analyzing the force evolution in time, a significant effect of the strain-rate sensitivity C on the force is noted. If the strain-rate sensitivity is low, for example $C = 0.0362$, two plastic collapses appear at the same time without oscillations of the force signal, Fig. 21(a). If the strain-rate sensitivity increases to $C = 0.3$ the collapse takes place at the impact side as it is shown in Fig. 20(d). In that case the dynamic yield stress is very high and prevents appearance of a buckling on the opposite side. Therefore, plastic strain accumulated during the round trip time of elastic wave propagation on the impact side leads to a collapse after two travels of the elastic wave when the reflection of the wave on the contact surface mass-crash-box appears. Therefore, the axial force in the crash box is controlled by the collapse force on the impact side and the loading level on the opposite side oscillates around the previous value, Fig. 21(b).

Based on the previous numerical observations the following conclusion may be drawn. According to Fig. 15, the collapse site process depends of the ratio between the yield stress levels observed in quasi-static loading ($\dot{\varepsilon}^{p} \approx 10^{-3}\,s^{-1}$) and in dynamic loading corresponding to $\dot{\varepsilon}^{p} \approx 10^{3}\,s^{-1}$. If the material is strongly strain-rate sensitive (low-quasi-static/dynamic yield stress ratio), no collapse is possible on the opposite side. This condition is satisfied if

$$\begin{cases} \left(1 + C \ln\left(\dfrac{\dot{\varepsilon}^{p}}{\dot{\varepsilon}_0}\right)\right) \geqslant 2, \\ C > 0.07 \end{cases}$$

$$\text{with} \quad \dot{\varepsilon}_0 = 10^{-3}\,s^{-1} \quad \text{and} \quad \dot{\varepsilon}^{p} = 10^{3}\,s^{-1}. \tag{8}$$

Another condition to trigger buckling on the impact side is to reach the stress amplitude higher than the quasi-static yield stress of the materials. Numerical simulations have been performed with new value of the constant A in Eq. (7a) satisfying this condition. The results are shown in Fig. 20(e) and (f). In that case, as expected, a collapse is seen on the impact side of the crash box.

Conversely, when a material is not rate sensitive Fig. 22(a), or showing negative strain-rate sensitivity like some kinds of aluminum alloys [35,36], the collapse will appear on the opposite side of impact and may induce bending of the structure especially for long structure [15,33,37]. In this case the desired high capacity of energy absorption of a structure to protect the passengers will be lost. Due to buckling of the structure, the force level will decrease. One can observe on the picture of a brass box (no strain-rate sensitivity) that the collapse took place near the embedded side of the specimen and not on the impact side. Recently, some results were reported in the literature for materials without strain-rate sensitivity, like those shown in Fig. 22 [36].

Experimental observation obtained for the material without strain-rate sensitivity confirms the numerical predictions and analysis concerning the role of the strain-rate sensitivity on the collapse phenomenon and the interaction between the plastic stress level induced by impact and the reflection of elastic waves from the clamp. Generally, in industrial practice of numerical calculations the trigger of collapse near the impact side is enforced until the buckling is similar to experiment. This problem appears also during numerical simulation using JC constitutive relation for materials with high yield stress and low strain-rate sensitivity.

A more precise modeling of the visco-plastic behavior of the material that would help to predict properly the collapse site is possible by accounting for the non-linear strain-rate sensitivity. Based on the Johnson–Cook

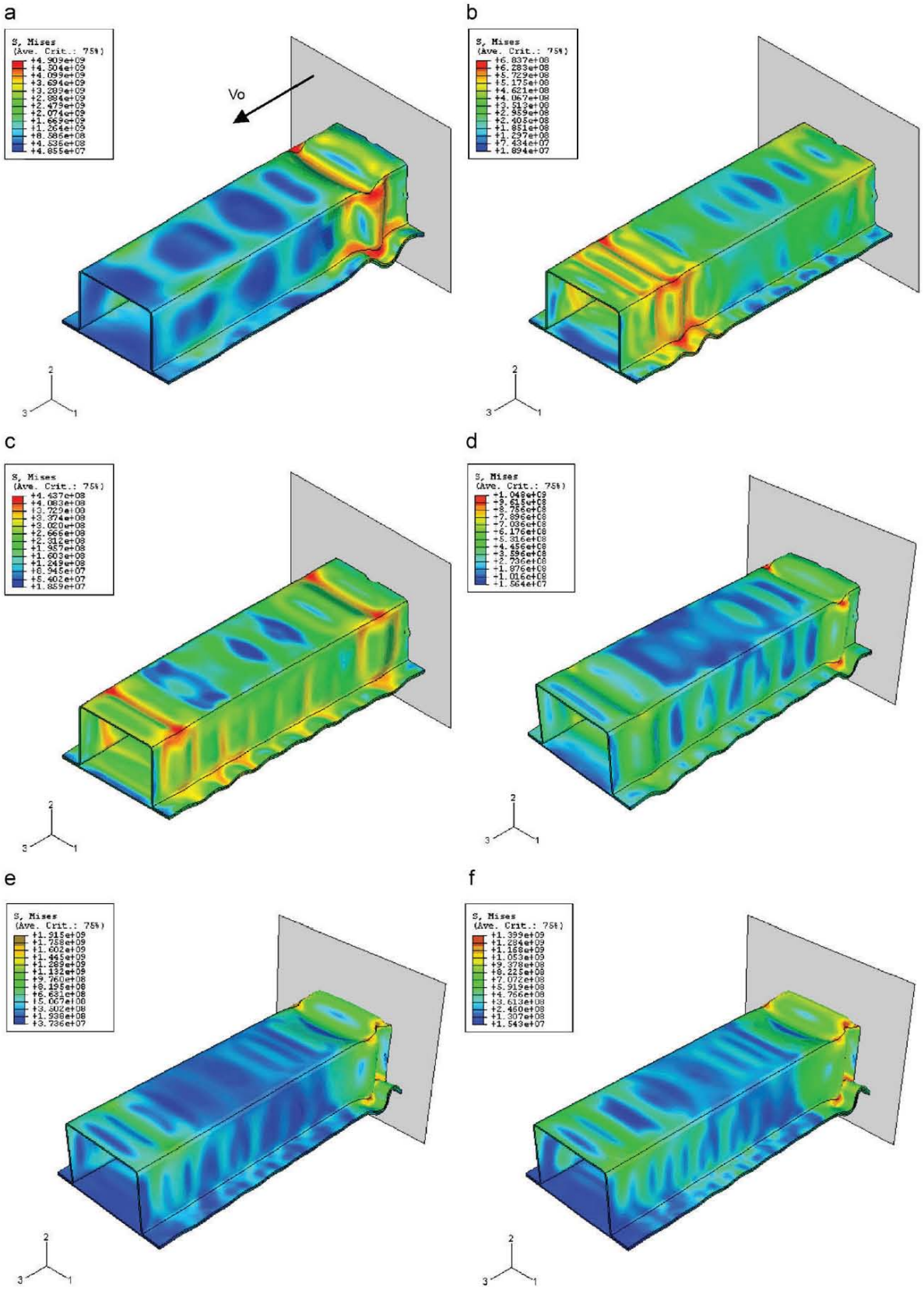

Fig. 20. Numerical simulations with JC constitutive relation and boundary conditions BC1, $V_0 = 16\,\text{m/s}$, $\mu = 0.1$ and $t_M = 3\,\text{mm}$. (a) Tool steel BC1, (b) 1006 steel BC1, (c) ES steel BC1, (d) ES steel with C = 0.12 BC1, (e) ES steel with C = 0.3 BC1, (f) ES steel with A = 200 MPa and C = 0.12 BC1.

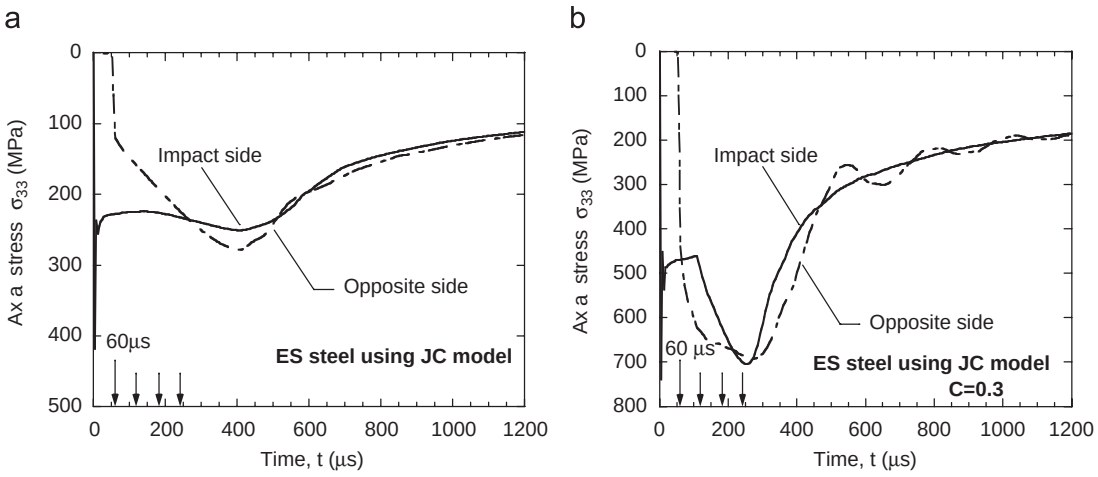

Fig. 21. Numerical predictions of forces for two strain rate sensitivities using BC1 and constants for mild steel ES: (a) rate sensitivity $C = 0.0362$; (b) rate sensitivity 0.3, for both cases $V_0 = 16\,\mathrm{m/s}$, $\mu = 0.1$ and $t_M = 3\,\mathrm{mm}$.

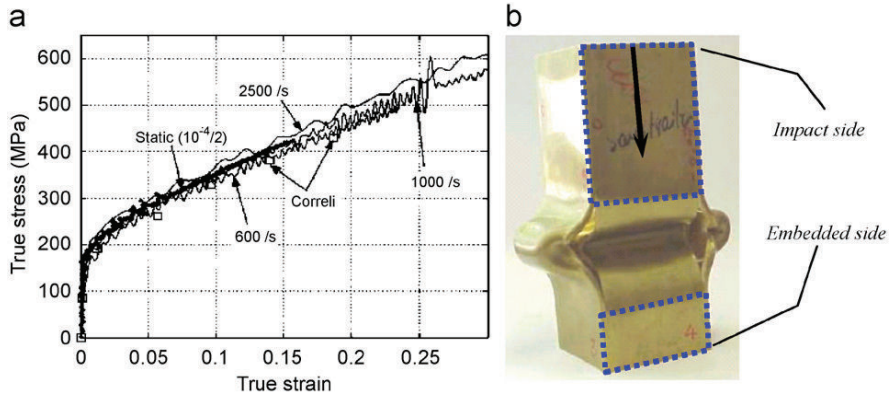

Fig. 22. (a) Strain rate sensitivity of brass (JC equation, $C \approx 0$) and (b) collapse of brass box, non rate sensitive material [36].

equation, an improvement already spotted in the literature for this problem [25,38,39] consist of adding a second term depending on $\dot{\varepsilon}^{\mathrm{p}}$, Eq. (9). Typically the rate sensitivity increases with strain rate, Fig. 4(a).

$$\sigma = (A + B(\varepsilon^{\mathrm{p}})^n)\left(1 + C_1 \ln\left(\frac{\dot{\varepsilon}^{\mathrm{p}}}{\dot{\varepsilon}_0}\right) + C_2\left(\ln\left(\frac{\dot{\varepsilon}^{\mathrm{p}}}{\dot{\varepsilon}_0}\right)\right)^2\right) \times \left(1 - \left(\frac{T - T_{\mathrm{room}}}{T_{\mathrm{melting}} - T_{\mathrm{room}}}\right)^m\right). \quad (9)$$

In the case of JC equation an improvement is to add one more term approximating the rate sensitivity. Simply, the second rate sensitivity can be introduced into Eq. (7). Therefore two constant rate sensitivities C_1 and C_2 govern in an artificial way the rate sensitivity. Although the improvement is introduced on pure phenomenological basis it may improve to some extent numerical evaluations of the crash-box analyses. An improvement may be expected in that case, notably around the transition point where the strain-rate sensitivity increases beginning from strain-rate $\dot{\varepsilon}^{\mathrm{p}} \geqslant 10\,\mathrm{s}^{-1}$. Of course, a correct solution in constitutive modeling is to introduce a complete constitutive relation with one non-linear term which approximates correctly the strain-rate sensitivity.

6. Conclusions

In this paper different numerical analyses of dynamic buckling and collapse of a crash box are reported taking into account both the elastic waves and plasticity effects. It has been observed that a strong competition exists between the elastic wave propagation and the local plasticity appearing during the first stage of impact. This competition defines the collapse site. In order to approximate correctly the buckling and collapse processes it is necessary to have a correct description of the strain-rate sensitivity of materials under consideration. The main idea is to assure a high plastic stress level under high strain rate to prevent any buckling on the opposite side of the crash box. This numerical study clearly indicates a problem if the material applied to design the crash box has in tension/compression close to zero or even negative, like Al alloys, strain-rate

sensitivity. High strength steels introduced recently into the automotive industry have such features.

Acknowledgment

The authors thank Prof. T. Lodygowski from Poznan University for the discussions and comments. The authors thank Arcelor Research Group and more precisely Dr. D. Cornette for his interest and recommendations for numerical calculations. The authors thank Prof. G. Ravichandran from Caltech for discussions and interest. The researchers of the University Carlos III of Madrid are indebted to the Spanish Ministry of Education (project DPI2005-06769), and to the Region of Madrid (project CCG06-UC3M/DPI-0796) for the financial support that allowed to perform a part of the numerical simulations.

References

[1] Durrenberger L, Even D, Molinari A, Rusinek A. Influence of the strain path on crash properties of a crash box structure by experi mental and numerical approaches. J Phys IV 2006;134:1287 93.
[2] Karagiozova D, Jones N. Dynamic elastic plastic buckling of circular cylindrical shells under axial impact. Int J Solid Struct 2000;37: 2005 34.
[3] Larour P, Verleysen P, Vermeulen M, Gomes MAR, Wedemeier A, Geoffroy JL, et al. Influence of pre straining and microstructure on the dynamic properties of high strength sheet steels. MS&T 2004 Conference Proceedings, New Orleans, USA, 2004. p. 171 83.
[4] Rusinek A, Klepaczko JR, Gadaj P, Nowacki WK. Plasticity of new steels used in automotive industries temperature measurements by thermo vision. SAE paper 2005 01 13626, 2005.
[5] Fischer FD, Reisner G, Werner E, Tanaka K, Cailletaud G, Antretter T. A new view on transformation induced plasticity (TRIP). Int J Plasticity 2000;16:723 48.
[6] Tomita Y, Shibutani Y. Estimation of deformation behavior of TRIP steels smooth/ringed notched specimens under monotonic and cyclic loading. Int J Plasticity 2000;16:769 89.
[7] Rusinek A, Zaera R, Klepaczko JR. Constitutive relations in 3 d for a wide range of strain rates and temperatures application to mild steels. Int J Solid Struct, 2007; doi:10.1016/j.ijsolstr.2007.01.015.
[8] Rusinek A, Klepaczko JR. Shear testing of s sheet steel at wide range of strain rates and a constitutive relation with strain rate and temperature dependence of the flow stress. Int J Plasticity 2001;17: 87 115.
[9] Haugou G, Markiewicz E, Fabis J. On the use of the non direct tensile loading on a classical split Hopkinson bars apparatus dedicated to sheet metal specimens characterisation. Int J Impact Eng 2006;8:778 98.
[10] Nowacki WK. Dynamic simple shear of sheets at high strain rates. In: Nowacki WK, Klepaczko JR, editors. New experimental methods in material dynamics and impact, series: trends in mechanics of materials, vol. 3; 2001. p. 309 36.
[11] Mouro P, Gary G, Zhao H. Dynamic tensile testing of sheet metal. J Phys IV 2000;49 54.
[12] Rusinek A, Zaera R, Klepaczko JR, Cheriguene R. Analysis of inertia and scale effects on dynamic neck formation during tension of sheet steel. Acta Mater 2005;53:5387 400.
[13] Awade A. CRASH AUTOMOBILE importance de la température et de l'anisotropie dans les essays dynamiques, Source RENAULT, Oral presentation. Proceeding MECAMAT, Aussois, France, 2005.
[14] Gloger S, Wanke T. Structural requirements and material selection in body development. In: von Hagen I, Wieland HJ, editors. Steels in cars and trucks. Wiesbaden/Germany. Dusseldorf/Germany: Verlag Stahleisen; 2005. p. 32 5.
[15] Karagiozova D, Jones N. Dynamic buckling of elastic plastic square tubes under axial impact II: structural response. Int J Impact Eng 2004;30:167 92.
[16] Rusinek A, Zaera R. Finite element simulation of steel ring fragmentation under radial expansion. Int J Impact Eng 2007;34: 799 822.
[17] Nemat Nasser S, Guo WG. Thermomechanical response of HSLA 65 steel plates. Mech Mater 2005;37:379 405.
[18] Molinari A, Ravichandran G. Constitutive modeling of high strain rate deformation in metals based on the evolution of an effective microstructural length. Mech Mater 2005;37:737 52.
[19] Johnson GR, Holmquist TJ, Anderson Jr. CE, Nicholls AE. Strain rate effects for high strain rate computations. J Phys IV France 2006;134:391 6.
[20] Zaera R, Fernandez Saez aJ. An implicit consistent algorithm for the integration of thermoviscoplastic constitutive equations in adiabatic conditions and finite deformations. Int J Solids Struct 2006;43: 1594 612.
[21] Zhao H, Abdennadher S, Othman R. An experimental study of square tube crushing under impact loading using a modified large scale SHPB. Int J Impact Eng 2006;32:1174 89.
[22] Song HW, Fan ZJ, Yu G, Wang QC, Tobota A. Partition energy absorption of axially crushed aluminium foam filled hat section. Int J Solid Struct 2005;42:2575 600.
[23] Kavi H, Kaan Toksoy A, Guden M. Predicting energy absorption in a foam filled thin walled aluminium tube based on experimentally determined strengthening coefficient. Mater Design 2006;27:263 9.
[24] Aktay L, Toksoy AK, Guden M. Quasi static axial crushing of extruded polystyrene foam filled thin walled aluminium tubes: experimental and numerical analysis. Mater Design 2006;27:556 65.
[25] Peixhino NRM. Study of visco plasticity models for the prevision of mechanical behaviour of high strength steels subjected to impact. Doctorat thesis, University of Minho, 2004 [Portugal].
[26] Ellobody A. Buckling analysis of high strength stainless steel stiffened and unstiffened slender hollow section columns. J Constructional Steel Research 2007;63:145 55.
[27] ABAQUS/Explicit User Manual volumes I and II, version 6.4.1, Hibbitt, Karlsson & Sorensen, Inc., 2004.
[28] Merle R. Mise en oeuvre d'un essai de double cisaillement en grandes déformations et sous solicitations dynamiques. Application à la caractérisation des tôles utilisées dans le crash automobile, Ph.D. thesis, LMT Cachan Paris, 2006.
[29] Song HW, Fan ZJ, Yu G, Wang QC, Tobota A. Partition energy absorption of axially crushed aluminum foam filled hat sections. Int J Solid Struct 2005;42:2575 600.
[30] Tam LL, Kurokawa T. Plastic buckling of cylinders by axial impact. In: Proceeding of the 1982 joint conference on experimental mechanics, vol. 2. JSME; 1982. p. 950 5.
[31] Kolsky H. An investigation of the mechanical properties of materials at very high rates of loading. Proc Phys Soc London 1949;62B: 676 700.
[32] Karagiozova D, Alves M, Jones N. Inertia effects in axisymmetrically deformed cylindrical shells under axial impact. Int J Impact Eng 2000;24:1083 115.
[33] Karagiozova D, Jones N. Influence of stress waves on the dynamic progressive and dynamic plastic buckling of cylindrical shells. Int J Solids Struct 2001;38:6723 49.
[34] Johnson G, Cook W. Fracture characteristics of three metals subjected to various strains, strain rates, temperatures and pressures. Eng Fract Mech 1985;21:31 48.
[35] Meguid SA, Attia MS, Stranart JC, Wang W. Solution stability in the dynamic collapse of square aluminium columns. Int J Impact Eng 2007;34:348 59.
[36] Zhao H, Abdennadher S. On the strength enhancement under impact loading of square tubes made from rate insensitive metals. Int J Solid Struct 2004;41:6677 97.

[37] Jensen Ø, Hopperstad OS, Langseth M. Transition from progressive to global buckling of aluminium extrusions a numerical study. Int J Crashworthiness 2005;10(6):609 20.
[38] Kang WJ, Cho S, Huh H, Chung DT. Modified Johnson Cook model for vehicle body crashworthiness simulation. Int J Vehicle Design 1999;21:424 35.
[39] Jeunechamps PP, Ponthot JP. An efficient implicit approach for the thermomechanical behaviour of materials submitted to high strain rates. J Phys IV 2006;134:515 20.
[40] Rusinek A, Klepaczko JR, Toth LS. Influence de l'échauffement adiabatique en régime adiabatique: application aux tôles d'acier. Revue Française de mécanique 2001;2:29 37.
[41] Plassart G, Philip G. Materials criteria selection and certification process for the body in white in PSA PEUGEOT CITROEN. SAE paper 2002 01 2051, 2002.
[42] Newsletter Arcelor Auto No. 3, Arcelor group, January 2003.
[43] Al Galib D, Limam A. Experimental and numerical investigation of static and dynamic axial crushing of circular aluminum tubes. Thin Wall Struct 2004;42:1103 37.
[44] Shim VPW, Yap KY. Modelling impact deformation of foam plate sandwich systems. Int J Impact Eng 1997;19:615 36.
[45] Bardenheier R, Rogers G. Dynamic impact testing with servohy draulic testing machines. J Phys IV France 2006;134:693 9.